Spine Deformity

www.spine-deformity.org

Spine Deformity 4 (2016) 182−192

Case Series

Morphometric Analysis of the Thoracic Intervertebral Foramen Osseous Anatomy in Adolescent Idiopathic Scoliosis Using Low-Dose Computed Tomography

Thorbjorn J. Loch-Wilkinson, MBBS, BSc, Maree T. Izatt, BPhty, Robert D. Labrom, MBBS, MSc, FRACS, Geoffrey N. Askin, MBBS, FRACS, Mark J. Pearcy, BSc, PhD, DEng, Clayton J. Adam, BEng, PhD*

Paediatric Spine Research Group, Queensland University of Technology and Mater Health Services Brisbane Ltd, Queensland, Australia

Received 9 November 2014; revised 15 September 2015; accepted 19 October 2015

Abstract

Purpose: The dimensions of the thoracic intervertebral foramen in adolescent idiopathic scoliosis (AIS) have not previously been quantified. Better understanding of the dimensions of the foramen may be useful in surgical planning. This study describes a reproducible method for measurement of the thoracic foramen in AIS using computed tomography (CT).

Methods: In 23 preoperative female patients with Lenke 1 type AIS with right-side convexity major curves confined to the thoracic spine the foraminal height (FH), foraminal width (FW), pedicle to superior articular process distance (P-SAP), and cross-sectional foraminal area (FA) were measured using multiplanar reconstructed CT. Measurements were made at entrance, midpoint, and exit of the thoracic foramina from T1−T2 to T11−T12. Results were also correlated with dependent variables of major curve Cobb angle measured on X-ray and CT, age, weight, Lenke classification subtype, Risser grade, and number of spinal levels in the major curve.

Results: The FH, FW, P-SAP, and FA dimensions and ratios are all significantly larger on the convexity of the major curve and maximal at or close to the apex. Mean thoracic foraminal dimensions change in a predictable manner relative to position on the major thoracic curve. There was no statistically significant correlation with the measured foraminal dimensions or ratios and the individual dependent variables. The average ratio of convexity to concavity dimensions at the apex foramina for entrance, midpoint, and exit, respectively, are FH (1.50, 1.38, 1.25), FW (1.28, 1.30, 0.98), FA (2.06, 1.84, 1.32), and P-SAP (1.61, 1.47, 1.30).

Conclusion: Foraminal dimensions of the thoracic spine are significantly affected by AIS. Foraminal dimensions have a predictable convexity-to-concavity ratio relative to the proximity to the major curve apex. Surgeons should be aware of these anatomical differences during scoliosis correction surgery.

Keywords: Adolescent idiopathic scoliosis; AIS; Morphometric; Intervertebral foramen; Computed tomography

Author disclosures: TJLW (none); MTI (travel allowances to institution from NuVasive; research support salary from Medtronic); RDL (received payment for speaking and/or teaching arrangements from Medtronic; research support salaries to institution from Synthes and Medtronic; grants to institution from DePuy Synthes in negotiation; fellowship support to institution from DePuy Synthes); GNA (received payment for speaking and/or teaching arrangements from Medtronic; research support salaries to institution from Synthes and Medtronic; grants to institution from DePuy Synthes in negotiation, all outside of submitted work); MJP (owns stock in Tissue Therapies; travel allowances to institution from NuVasive; holds scientific advisory board or other office from Therapeutics Goods Administration, Australia); CJA (travel allowances to institution from NuVasive; research support salaries and materials to institution from Synthes and Medtronic; grants to institution from DePuy Synthes in negotiation; fellowship support from European Union Fellowship FP7-PEOPLE-2010-IIF-274964 salary 2012-13, all outside of submitted work).

No funds were received in support of this work. No benefits in any form have been or will be received from a commercial party related directly or indirectly to the subject of this manuscript.

*Corresponding author. Paediatric Spine Research Group Centre for Children's Health Research, Level 5, 62 Graham Street, South Brisbane, Queensland 4104, Australia. Tel.: +61 7 3069 7324.

E-mail address: c.adam@qut.edu.au (C.J. Adam).

2212-134X/$ - see front matter © 2016 Scoliosis Research Society.
http://dx.doi.org/10.1016/j.jspd.2015.10.004

Introduction

Deformation of the posterior elements and asymmetrical growth of the posterior elements relative to the vertebral body are an important morphological aspect of adolescent idiopathic scoliosis (AIS) [1] and have been described in other anatomical studies [2-4]; however, the quantitative effects of this deformity on the thoracic intervertebral foramen in AIS have not previously been described. Accurate and reproducible study of the intervertebral foramen in scoliosis is difficult because of the three-dimensional nature of the deformity. The foramen also is a complex three-dimensional space that is affected by the deformity of the individual vertebral elements that form its boundaries. The clinical relevance of the dimensions of the thoracic intervertebral foramen at this stage are uncertain; however, an improved understanding of the differences in convexity and concavity intervertebral foramina may be of benefit to surgeons or other clinicians in assessing the local anatomy in individual patients with AIS, or in future advances in implant development.

Some controversy exists in the precise definition of the intervertebral foramen; however, it is usually considered to be bounded by vertebral body and posterior element osseous structures, including the pedicle superiorly and inferiorly, the pars and zygapophysial joints and ligamentum flavum posteriorly, and the vertebral body and disc anteriorly [5]. The foramen is a complex three-dimensional shape with an entry and exit bounded by the medial and lateral borders of the pedicles. Although anatomical studies have been performed of the vertebrae and specific parts of the posterior elements in normal [6-9] and deformed spines [3,10-12], only a limited number of studies have included the intervertebral foramen and are more numerous for the cervical [13,14] and lumbar regions [5,15-20]. A literature search by the authors found no quantitative studies of the thoracic spine intervertebral foramen in normal or AIS patients. Studies of the intervertebral foramen of the cervical and lumbar spine describe or depict in example pictures different anatomical landmarks and methods of measurement that make comparison and reproduction difficult. Deformity measurements such as axial rotation or coronal tilt that are relevant to morphometric spine studies such as this are also heterogeneous and have inherent problems in reproducibility of measurement [21,22]. This study, therefore, was undertaken to better understand the dimensions of the thoracic intervertebral foramen in AIS as a contribution to the anatomical literature and as a potential aid to surgical planning.

Materials and Methods

Twenty-three CT scans with the highest image quality were selected from an existing historical databank of low-dose CT scans of preoperative patients with AIS who subsequently underwent thoracoscopic scoliosis correction surgery. The databank contained scans collected between the years 2002 and 2009; however, the selected scans for the current study were those most recently taken between 2007 and 2009. All scans in the Preop CT Databank are from an Australian surgical practice of two experienced spinal orthopaedic surgeons (RDL and GNA) in Brisbane, Queensland. Low-dose CT spine scans covering C7 to S1 had been collected as part of a routine preoperative protocol for surgical planning purposes during those years, though they are no longer performed as part of current practice. The compilation and use of the databank for future research projects has ethics approval from our institution's Human Research Ethics Committee. Scans were performed in the supine position on Brilliance 64 and Lightspeed VCT machines with X-ray source voltage and current of 80–100 kVp and 29–119 mA, respectively, and a slice thickness of 2.5–3 mm with 1–1.25 mm overlap between slices, giving voxel dimensions ranging between 0.49 × 0.49 × 1 mm and 0.78 × 0.78 × 1.25 mm. The scans from the databank used in this study had an average estimated

Table 1
Demographic data of patients.

Characteristics of Study Group (n = 23)	Mean
Age (years)	15.7 (11.6–22.0)
Weight (kg)	55.2 (37.5–84.7)
Race	55.2 (37.5–84.7)
Major Cobb angle—X-ray measured (degrees)	53.7 (42–63)
Major Cobb angle—CT measured (degrees)	43.5 (34.5–53)
	Number of patients
Race	
Caucasian	22 (96%)
Polynesian	1 (4%)
Lenke classification	
1A	13
1B	4
1C	6
Risser grade	
0	3
1	0
2	1
3	3
4	8
5	8
Apex level	
T7	2
T7–T8	4
T8	2
T8–9	7
T9	3
T9–T10	5
No. of spinal levels in major curve	
5	1
6	3
7	13
8	5
9	1
Mean	7.08

Note: Means are given with (ranges).

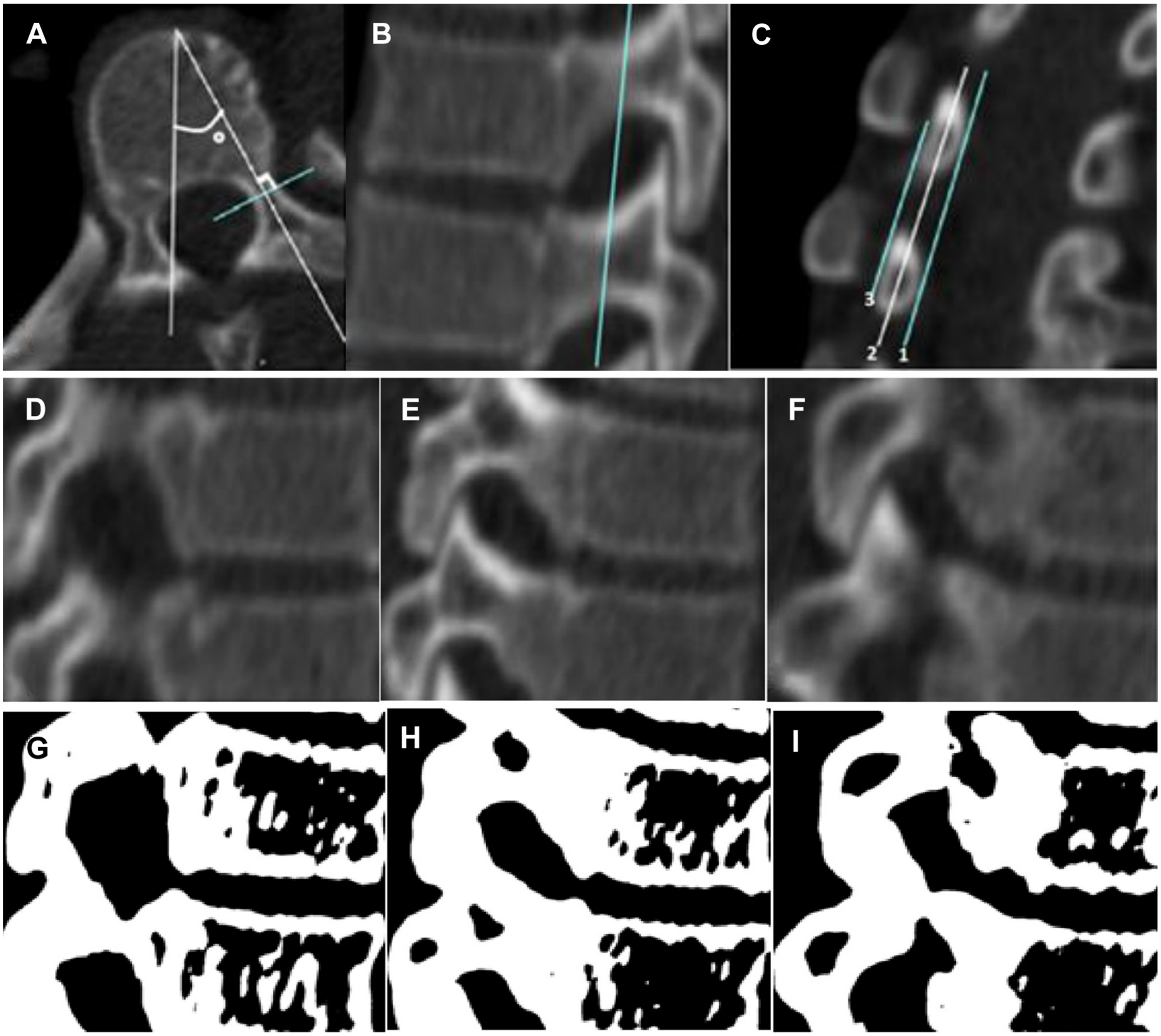

Fig. 1. Image acquisition. (A) Calculation of pedicle angle relative to vertical orientation of true axial plane. The axial plane was then corrected to a mean of adjacent level angles. (B) The sagittal plane axis was adjusted in line with adjacent pedicle isthmuses. (C) The coronal planes were adjusted for (1) the foraminal entrance; (2) the foraminal midpoint; and (3) the foraminal exit. (D) Image of foraminal entrance at 800 HU center and 2,000 HU width. (E) Image of foraminal midpoint at 800 HU center and 2,000 HU width. (F) Image of foraminal exit at 800 HU center and 2,000 HU width. (G) Thresholded image of foraminal entrance at 300 HU center and 0 HU width. (H) Image of foraminal midpoint at 300 HU center and 0 HU width. (I) Image of foraminal exit at 300 HU center and 0 HU width.

radiation dose of approximately 2 mSv. The scans were analyzed using Carestream® PACS viewer software (Rochester, NY) with a multiplanar reconstruction function (MPR) with a double oblique function setting. The reported accuracy of the measurement tools in the program was 0.01 mm.

The demographic data of the selected patients are described in Table 1. Inclusion criteria included a diagnosis of AIS, female gender, Lenke 1 type curve, and a major scoliosis curve confined to the thoracic spine. Exclusion criteria included non-AIS scoliosis, non−Lenke 1 type scoliosis, male gender, and where the major curve included the lumbar spine.

All Cobb angle measurements, Risser grading, and Lenke classification were performed by the same two orthopaedic surgeons who subsequently performed the surgery.

This study did not have a control group, as scoliotic age-matched cadaver controls or cadaveric scoliosis specimens do not exist. Ethics approval was not possible to utilize nonscoliosis spinal CT scans either retrospectively, because of privacy reasons, or prospectively, as studies would involve unnecessary radiation exposure. With regard to the use of CT for anatomical measurements, other studies in non-AIS patients have demonstrated good correlation between CT measurements in spinal anatomy compared to

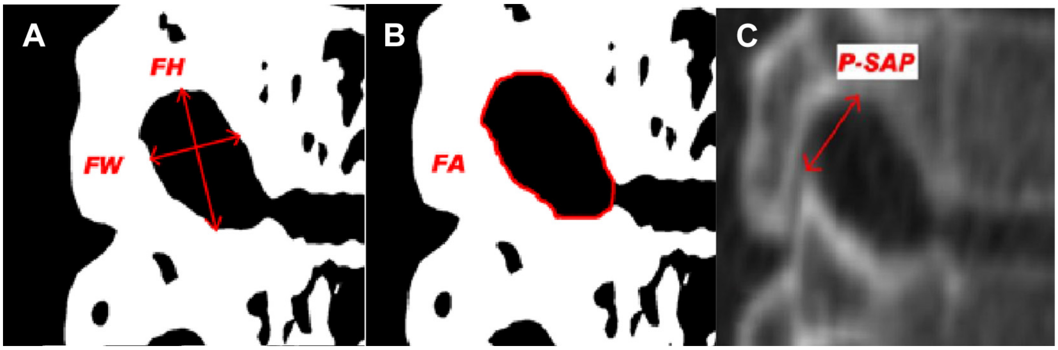

Fig. 2. Measurement of anatomical landmarks. (A) Foraminal Height (FH) was measured from between the inferior cortex of the upper pedicle isthmus and superior cortex of the lower pedicle isthmus. Foraminal width (FW) was measured orthogonal to the FH commencing from a point along the posterior aspect of the vertebral body equidistant between the junction of the inferior aspect of the upper pedicle and the vertebral body and the most posterior aspect of the inferior endplate of the same vertebral body and measured to the nearest osseous border. These measurements were done with 300HU Centre and 0HU Width. (B) Foraminal Area (FA) was measured using a manual cursor method using the osseous boundaries of the foramen. These measurements were done with 300HU Centre and 0HU Width. (C) Pedicle to Superior Articular Process Distance (P-SAP) was measured from the tip of the superior articular process (SAP) to the same point measured on the inferior cortex of the pedicle isthmus already measured in A. Use of the extended window settings of 800HU centre and 2000 HU width was necessary to more accurately estimate the location of the tip of the SAP.

direct measurements of anatomy using cadaveric specimens [20,23-25].

Image Acquisition Using Multiplanar Reconstruction and Thresholds

A depiction of the image acquisition can be found in Figure 1. Each scan was initially viewed in an MPR format using a grayscale window centered about 800 Hounsfield units (HU) with a width of 2,000 HU (ie, a range of −200 to 1,800 HU). Angles of the pedicles relative to the vertical orientation in a true axial plane were measured using an angle-measuring function with a line bisecting the pedicle isthmus (see Fig. 1A). All measurements were taken twice by the same observer and averaged. The axial plane orientation was then adjusted to a mean of the measured pedicle angle for adjacent pedicles. This adjustment corrected for the axial plane rotational deformity. This method of axial plane correction is different from published methods of estimating axial plane rotational deformity of vertebrae that utilize a mean of vertebral body rotation angles [15]. However, an axial plane correction that utilized the local anatomy of the pedicles comprising the superior and inferior border of the foramen was felt by the authors to be more anatomically correct when analyzing the foramen and allowed for potential asymmetry of the posterior elements. This method was also found to better align with the orientation of the foramen in pilot studies undertaken by the authors and in particular allowed better visualization of the foraminal exit.

The sagittal plane axis was orientated into an oblique plane that bisected each adjacent pedicle isthmus (see Fig. 1B). This corrected for the sagittal plane deformity and allowed the coronal plane subsequently to be adjusted with visualization of an imaging plane through both pedicle isthmuses. The axial and sagittal planes were thereafter not altered, and only the coronal plane adjusted for measurements of the entrance, exit, and foramen.

Before adjusting the coronal plane to obtain the final image, the image settings were changed to a window center of 300 HU and a window width of 0 HU (see Fig. 1G–I). This provided a thresholded binary image whereby all white borders were assumed to be osseous structures. This was necessary as the low-dose protocols used in the CT scans had a high noise–signal ratio, and wider window settings created an indistinct osseous margin at the high magnifications required to measure the foramen. Setting a threshold of 300 HU appeared appropriate as this is typically the lower limit of bone and the upper limit of soft tissue. A Hounsfield unit threshold of 300 has been found to correlate best with cadaveric controls in a previous CT study by Smith et al. measuring intervertebral foramina in the lumbar spine [20] and appeared to be most correct anatomically in a pilot study undertaken by the authors when compared to other published thresholds that were found to be unsuitable with this CT series.

After thresholding, the coronal plane was adjusted to generate images of the entrance, midpoint, and exit of the foramen (see Fig. 1C–I). An image of the entrance of the foramen was obtained by adjusting the coronal plane to align with the medial surface of adjacent pedicles at the isthmus (see Fig. 1C-1). A similar method has been previously described by Kaneko et al. [15]. The entrance was defined as the most medial point at which an uninterrupted bridge of bone could be visualized for both upper and lower pedicles between the vertebral body and pars interarticularis (see Fig. 1C-1, D, and G). An image of the midpoint of the foramen was obtained

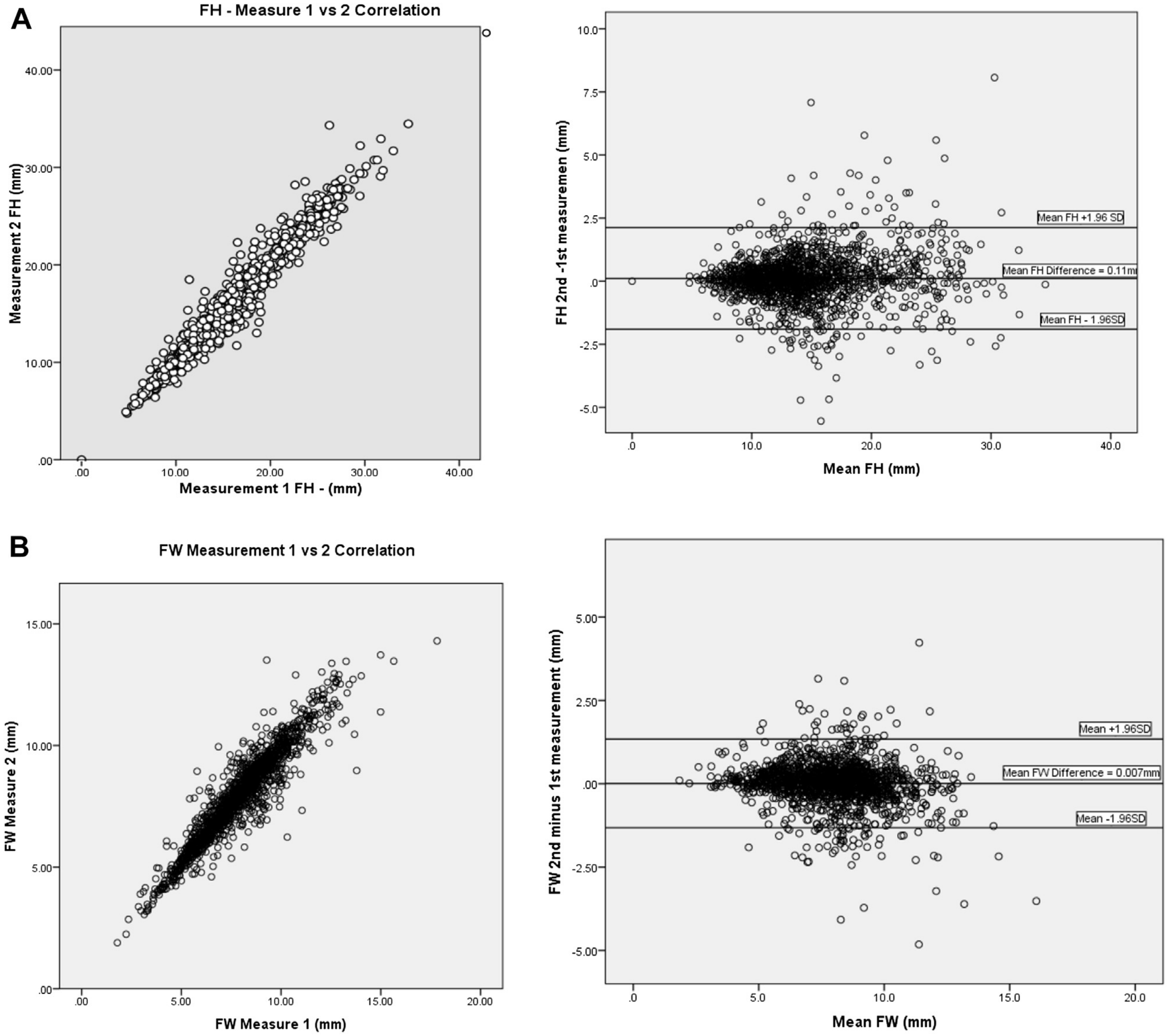

Fig. 3. Intraobserver variability. Repeat measurements were correlated and compared using the 95% limits of agreement method as described by Bland and Altman for (A) FH, ratio R:L FH ±1 SD vs. apex level; (B) FW, ratio R:L FW ±1 SD vs. apex level; (C) FA, ratio R:L FA ±1 SD vs. apex level; and (D) P-SAP, ratio R:L P-SAP distance ±1 SD vs. apex level. R:L, right−left; FH, foraminal height; SD, standard deviation; FW, foraminal width; FA, foraminal area; P-SAP, pedicle to superior articular process distance.

by scrolling the imaging plane laterally and then adjusting the oblique coronal plane to bisect the width of the upper and lower pedicle isthmus (see Fig. 1C-2, E, and H). This was necessary as adjacent pedicles were often of different thickness and therefore required a plane correction. The exit of the foramen was measured using an oblique coronal plane that best aligned with the inferolateral border of the upper pedicle and the superolateral border of the lower pedicle (see Fig. 1C-3, F, and I). This was necessary as the lateral surface of the pedicle was typically concave and varied in morphology. The exit of the foramen was defined as being the point as lateral as possible, where the borders of the foramen including vertebral body, pedicles, pars, and zygapophyseal joints could still be visualized in continuity (see Fig. 1F and I).

Anatomical Measurements

All measurements were undertaken using osseous anatomy. Although ligamentous structures including the ligamentum flavum are considered to comprise the posterior border of the intervertebral foramen, the CT studies utilized in this study were low-dose CT scans originally intended for surgical planning and had a high noise−signal ratio with significant artifact at the high magnifications used to visualized the foramen and thus were not suitable for reliably measuring soft tissue anatomy. Measurements therefore were to the osseous anatomical boundaries. All measurements were undertaken by a single researcher (TLW) and were repeated at an interval of 6 weeks, with blinding to the first results. Anatomical measurements were defined as follows and are demonstrated in Figure 2.

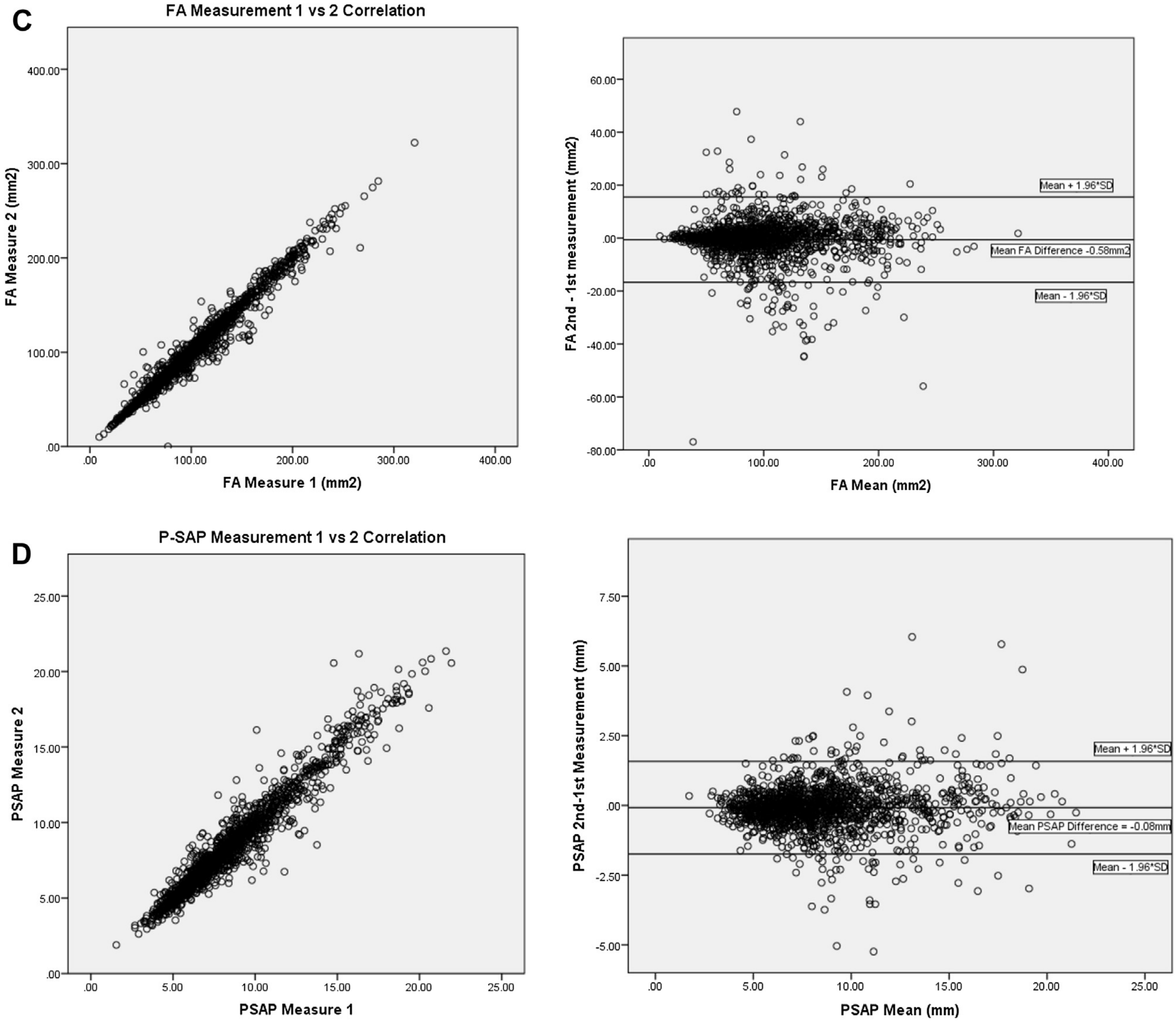

Fig. 3. (*continued*).

Foraminal Height

An example of foraminal height (FH) measurement is given in Figure 2A. Foraminal height was defined as the distance between the inferior cortex of the upper pedicle isthmus and superior cortex of the lower pedicle isthmus. This allowed measurement using a consistent anatomical point, rather than using the axes of the shape of the foraminal area, which varied considerably between individuals. Use of these landmarks was consistent with the described or graphically depicted definition of foraminal height in lumbar spine studies [5,15-17,20].

Foraminal Width

An example of foraminal width (FW) measurement is given in Figure 2A. The foraminal width was measured orthogonal to the foraminal height measurement commencing from a point along the posterior aspect of the vertebral body equidistant between the junction of the inferior aspect of the upper pedicle and the vertebral body and the most posterior aspect of the inferior endplate of the same vertebral body and measured to the nearest osseous border. This posterior limit of measurement usually lay close to either the tip of the superior articular process or along the anterior margin of the inferior articular process. Landmarks used for measurements of foramen width vary in other anatomical studies; however, use of those described here appeared to be similar to the examples given in a lumbar spine study by Kaneko et al. [15].

Foraminal Area

An example of the foraminal cross-sectional area (FA) is given in Figure 2B. Foraminal area was measured using a manual cursor method encircling the margin of the posterior vertebral body, inferior border of the upper pedicle, the anterior margin of the inferior articular facet of the upper vertebra, of the anterior border of the superior articular facet of the lower vertebra, and the superior border of the lower pedicle. To account for the border of the posterior disc annulus, which could not always be clearly visualized, an assumption was made that the border of the disc was defined by a line drawn from the point of inflexion between posterior vertebral body and inferior endplate in an orientation orthogonal to the orientation of the adjacent endplates and extending to the nearest osseous point caudally (see Fig. 2B). This was always at the most posterior aspect of the superior endplate of the more caudal vertebral body.

Pedicle to Superior Articular Process Distance

An example of the pedicle to superior articular process distance (P-SAP) is given in Figure 2C. The P-SAP distance was measured from the tip of the superior articular process to the same point along the inferior aspect of the upper pedicle that was used to measure foraminal height (see Fig. 2A). Use of the inferior cortex of the pedicle isthmus as a measurement landmark for P-SAP distance is similar to that given in the diagrams depicted in a recent study of the intervertebral foramen in degenerative lumbar scoliosis [15]. Use of the extended window settings of 800 HU center and 2,000 HU width was used to more accurately identify the tip of the SAP, which was sometimes obscured at the setting of 300 HU center and 0 HU width used for other measurements.

Theory and Calculation

Statistical Methods

The Pearson correlation coefficients were calculated for the repeated measurements of FH, FW, FA, and S-SAP distance. Mean difference and 95% limit of agreement analysis was also performed following Bland and Altman [26].

Data were also grouped to correspond to the spinal level relative to the apex of the major curve, with the apex level designated as zero, rostral levels given sequential negative values, and caudal levels given sequential positive values. Where the apex level was a single vertebral level, that is, T8, the apex foramina was assumed to be the more rostral foramina, that is, T7–T8. Individual left- and right-side foraminal measurements were also combined to give a ratio of right–left sides.

Linear regression was performed using the statistical program SPSS (version 21, IBM Corp, Armonk, NY) comparing regressing dependent variables FH, FW, FA, and P-SAP right–left side ratios against the following potential independent variables; major curve Cobb angle measured on X-ray and CT, age, weight, Lenke classification, Risser grade, and number of spinal levels in the major curve. A p value $<.05$ was considered statistically significant.

Results

Mean results according to anatomical level are summarized in Table 2. From the 23 scans, measurements could be performed on almost all foramina except for a single T1–T2 foramen as a result of excessive noise (poor resolution). The midpoint of a single right-side T11–T12 foramen and of the exit points of 6 of the 23 right-side T11–T12 foramina could not be accurately assessed with the protocol because of the anatomical variations of pedicle and facet joint morphology caused by the changes from thoracic to lumbar type morphology. The total number of measurements for FH, FW, FA, and P-SAP were 1,500, 1,498, 1,498, and 1,500, respectively.

Pearson correlation coefficients comparing repeat measurements were 0.98, 0.94, 0.98, and 0.97 for FH, FW, FA, and P-SAP, respectively. Mean difference between measurements were 0.11 mm, 0.007 mm, −0.58 mm^2, and −0.08 mm, with standard deviations of 1.03 mm, 0.68 mm, 8.22 mm^2, and 0.84 mm for FH, FW, FA, and P-SAP, respectively. Figures demonstrating correlation between measurements and 95% limits of agreement as described by Bland and Altman [26] are given in Figure 3. These demonstrated a high level of intraobserver reproducibility.

Comparison of Dimensions Between Convexity (Right Side) and Concavity (Left Side) of Major Thoracic Curve

The right–left ratios averaged for all spinal levels relative to the apex are presented in Figure 3A–D; all figures include error bars ± 1 standard deviation. At the apex level where differences were expected to be maximal, the right–left ratios for foraminal entrance, midpoint, and exit, respectively, for the four measurements were FH (1.50, 1.38, 1.25), FW (1.28, 1.30, 0.98), FA (2.06, 1.84, 1.32), and P-SAP (1.61, 1.47, 1.30), demonstrating that, with the exception of FW at the exit, all apical measurements were larger on the convexity (right) side. The differences in ratio decreased from entrance to midpoint to exit with the exception of foraminal width, which was slightly greater at the midpoint than at the entrance.

No statistically significant correlation was found between foraminal dimensions or their right–left ratios and the candidate independent variables described previously.

Table 2
Summary of mean measurements using anatomical level measured with ± 1 standard deviation for FH, FW, P-SAP, and FA on right (R) and left (L) side and entrance, midpoint, exit of the foramen for T1−T2 to T11−T12.

	Foramen region	Side	FH (mm)	FW (mm)	FA (mm^2)	P-SAP (mm)
T1−T2	Entrance	R	16.0±1.4	6.9±1.1	88.7±14.8	7.9±1.0
		L	18.3±2.0	7.5±1.4	115.4±25.2	8.7±1.6
	Midpoint	R	7.4±2.1	5.5±1.2	39.4±13.0	4.3±0.7
		L	8.4±1.8	6.0±1.8	48.3±19.9	4.7±1.3
	Exit	R	10.8±1.2	6.9±1.5	67.4±18.1	5.6±1.0
		L	12.0±1.8	7.8±2.0	83.4±23.9	6.6±1.2
T2−T3	Entrance	R	15.0±1.6	7.0±1.1	77.8±15.1	7.6±1.0
		L	19.7±1.7	8.7±1.0	139.5±17.7	10.8±1.9
	Midpoint	R	7.8±1.4	5.4±1.4	37.6±12.5	4.6±0.9
		L	9.8±1.5	6.2±1.3	58.4±14.4	5.3±0.9
	Exit	R	11.3±1.5	6.8±1.5	63.6±14.1	6.3±1.0
		L	13.3±1.8	8.1±1.2	91.6±21.5	7.9±1.3
T3−T4	Entrance	R	15.0±2.0	7.4±0.8	81.0±14.1	8.2±1.5
		L	19.6±1.7	9.3±1.2	147.9±24.2	11.2±1.3
	Midpoint	R	8.5±1.2	6.3±1.1	49.1±13.1	5.4±0.8
		L	10.6±1.3	6.6±1.3	68.3±14.7	5.9±1.0
	Exit	R	10.7±1.5	7.4±1.2	67.7±13.6	6.5±0.9
		L	13.9±2.0	8.2±1.1	95.0±21.0	8.3±1.3
T4−T5	Entrance	R	16.4±2.8	8.3±0.8	103.1±23.0	8.9±2.2
		L	19.0±2.3	9.7±1.3	147.7±29.8	11.4±1.5
	Midpoint	R	9.4±1.5	7.1±1.1	61.9±17.8	6.1±1.1
		L	11.6±1.4	6.8±1.4	75.8±17.0	6.6±1.2
	Exit	R	11.1±1.3	7.6±1.3	73.3±18.7	7.2±1.2
		L	14.6±1.5	8.2±1.1	97.9±18.2	8.8±1.3
T5−T6	Entrance	R	18.5±2.5	9.7±0.9	138.1±28.3	10.3±1.9
		L	17.5±1.7	9.7±1.3	129.9±28.8	10.5±1.4
	Midpoint	R	10.5±1.4	7.5±1.1	75.4±16.7	6.6±1.2
		L	11.7±1.4	6.9±1.4	73.1±15.2	6.8±1.4
	Exit	R	12.0±1.2	7.7±1.1	80.5±16.4	7.8±1.3
		L	14.3±1.5	8.3±1.3	95.0±15.6	9.0±1.5
T6−T7	Entrance	R	21.6±2.4	10.7±1.2	173.8±31.1	12.6±1.9
		L	16.4±1.8	9.0±1.2	113.4±26.3	9.8±1.4
	Midpoint	R	11.8±1.6	7.6±1.4	88.4±20.3	6.9±1.4
		L	11.4±1.6	6.7±1.7	68.0±14.4	6.6±1.4
	Exit	R	13.6±1.9	7.8±1.2	93.2±19.6	8.6±1.6
		L	13.9±1.5	8.2±1.5	91.5±16.9	8.6±1.5
T7−T8	Entrance	R	23.0±2.3	10.9±1.6	195.1±27.8	14.1±1.6
		L	16.5±2.1	8.5±1.1	107.5±21.1	10.0±1.7
	Midpoint	R	12.8±1.3	8.0±1.4	100.8±20.2	7.4±1.4
		L	11.0±1.6	6.8±1.6	65.2±17.5	6.4±1.3
	Exit	R	15.0±1.6	8.1±1.1	102.4±18.1	9.4±1.6
		L	14.2±1.7	8.5±1.8	94.4±18.4	8.7±2.0
T8−T9	Entrance	R	24.3±1.9	10.3±1.5	198.3±21.2	15.5±1.9
		L	16.5±2.1	8.2±1.1	101.6±20.2	9.3±1.6
	Midpoint	R	13.4±1.0	8.0±1.5	103.3±16.0	7.9±1.5
		L	9.9±2.0	6.0±1.5	55.4±17.4	5.2±1.0
	Exit	R	15.0±1.3	7.7±1.2	102.8±15.9	8.9±1.3
		L	12.2±1.8	7.6±2.0	76.7±21.0	6.9±1.5
T9−T10	Entrance	R	24.2±3.0	9.1±1.7	183.4±31.9	15.5±1.7
		L	18.3±2.9	8.4±1.1	111.9±26.1	10.2±2.1
	Midpoint	R	13.1±1.1	7.7±1.7	94.9±18.8	7.6±1.3
		L	9.8±1.9	5.8±1.4	56.9±18.3	5.1±1.0
	Exit	R	14.7±1.0	8.2±1.4	112.3±18.3	8.6±1.3
		L	11.7±1.8	7.8±1.9	87.9±25.8	6.8±1.4
T10−T11	Entrance	R	24.7±2.3	8.1±1.5	174.4±29.5	16.0±1.8
		L	21.6±3.7	8.2±1.3	140.2±37.3	12.6±2.7
	Midpoint	R	14.1±1.1	7.8±1.8	98.4±18.6	8.1±1.7
		L	11.1±1.9	7.3±1.7	74.2±20.8	6.4±1.3
	Exit	R	15.3±1.4	9.0±1.5	129.2±23.2	9.4±1.7
		L	13.2±1.9	9.0±1.8	109.8±23.8	8.5±1.4
T11−T12	Entrance	R	25.8±2.7	8.7±1.8	187.2±37.5	16.9±2.2
		L	27.5±3.5	8.8±1.9	202.3±50.5	16.7±2.7
	Midpoint	R	14.3±1.5	8.5±2.0	114.9±24.9	8.0±2.1
		L	13.3±1.9	9.9±2.1	121.3±35.5	8.2±1.9
	Exit	R	15.9±1.6	9.7±2.4	141.9±41.1	9.7±2.6
		L	15.2±1.6	11.4±2.0	163.1±35.1	10.1±1.8

(Continued)

Table 2 (Continued)

R, right; L, left; FH, foraminal height; SD, standard deviation; FW, foraminal width; FA, foraminal area; P-SAP, pedicle to superior articular process distance.

Discussion

This anatomical study quantified thoracic foraminal dimensions for a group of AIS patients based on measurements from low-dose preoperative CT scans. A marked asymmetry in foraminal dimensions was found in the vicinity of the scoliotic major curve apex, with right-side dimensions being up to twice the left-side dimensions. Away from the curve apex, right−left foraminal dimension ratios behaved in a predictable manner relative to the distance above or below the apex. The ratio of right−left was always maximal at or within one level of the apex and was close to 1:1 typically 3 levels above or below the apex. This was to be expected given the most common number of levels involved in the major thoracic curve was 7 (see Table 1). Thus, in a ‘‘typical’’ AIS spine with an apex at the level at T7−T8 with involvement of seven spinal levels in the major thoracic curve, the foraminal dimensions would be expected to be approximately equal at either T4−T5 or T5−T6 and at T10−T11 or T11−T12. Of note in this study, differences between right−left foraminal dimension ratios decrease in magnitude as the foramen proceeds laterally from entrance to midpoint to exit. A possible explanation for this is remodeling of the pedicle, although measurement of pedicle dimensions were beyond the scope of this study and has been examined in other studies [2,4]. The results of this study suggest that the asymmetry in foraminal dimensions in AIS is primarily a function of the coronal curvature of the spine (in particular, proximity to the apices of the coronal spinal curves) rather than asymmetry of the posterior elements. Further evidence of this is that the foraminal height, and pedicle−superior articular process, appear to change more substantially than foraminal width in relation to the curve apex (see Fig. 4A−C).

No statistically significant correlation was found between right−left foraminal dimension ratios and the major Cobb angle, which was unexpected as a larger curve would theoretically be expected to increase the differences between convexity and concavity foramina. A possible explanation for this is that the sample of spines in this group comprised a relatively homogenous group because of the obvious selection bias of preoperative patients. All

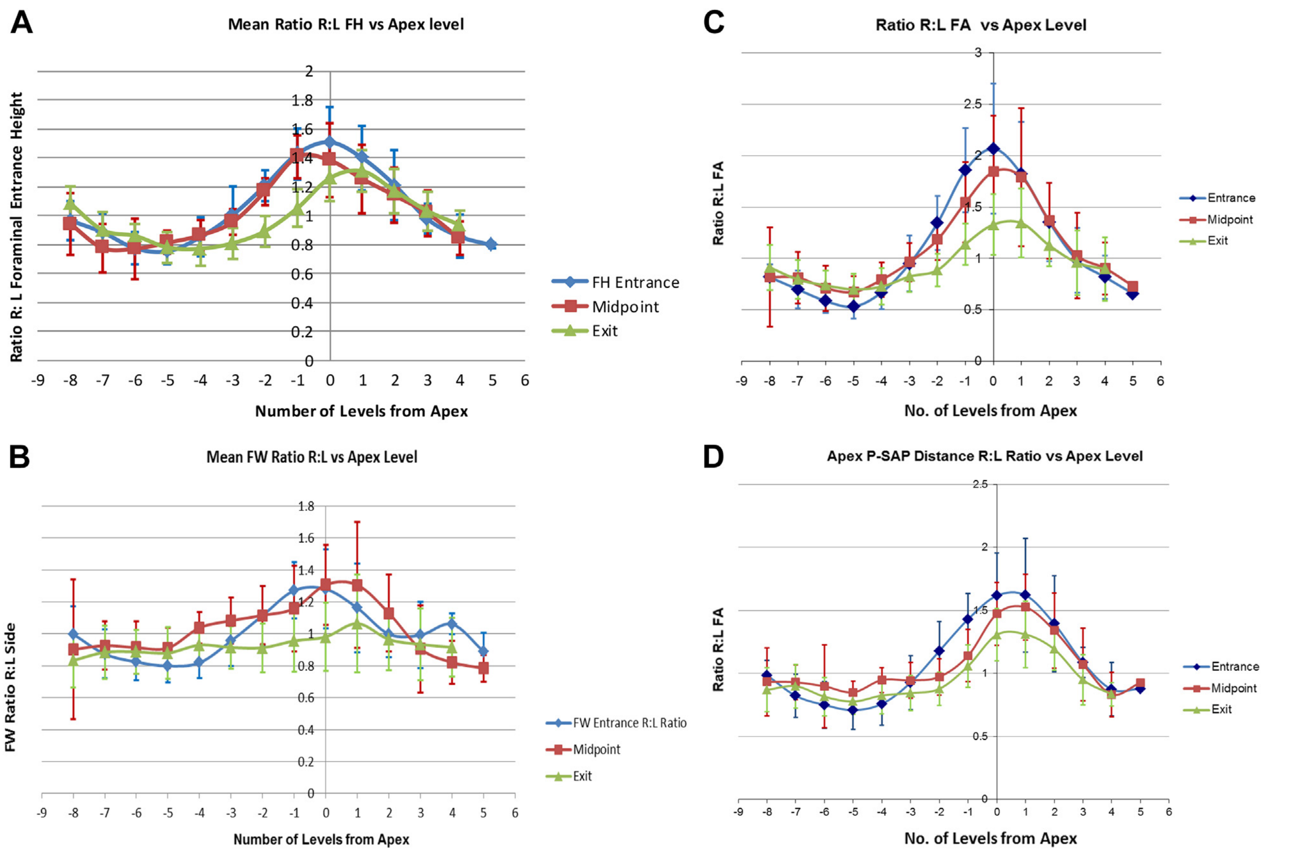

Fig. 4. (A−D) Ratio of right−left foraminal dimensions for (A) foraminal height (FH); (B) foraminal width (FW); (C) foraminal area (FA); and (D) pedicle to superior articular process distance (P-SAP) vs. vertebral level relative to the apex level of the major thoracic curve. Error bars for all figures are ±1 standard deviation.

patients had major Cobb angles within 21 degrees of each other on X-ray measurements and within 20 degrees on CT measurement, and there were no curves less than 34 degrees; therefore, the evolution of foraminal asymmetry during scoliosis progression cannot be inferred from the current patient group. A statistically significant difference may exist with a larger sample size or inclusion of more severe scoliosis cases with larger curves, which could be the subject of further study.

A limitation of this study was that a control group of age-matched typically developing subjects could not be included ethically. Such control scans would, in any case, have been unlikely to account for potential differences such as osteopenia, which is a feature of AIS [27], and is relevant to selection of appropriate Hounsfield unit thresholds for measurement in CT studies. In addition, it was not possible to compare radiologic measurements with physical specimens, as cadaveric specimens for this age group are generally not available. Use of adult cadaveric spines would not have been appropriate given potential differences in bone quality and degenerative changes. The quality of the CT data was low as the original purpose of the scans had been for surgical planning purposes with a minimum of radiation exposure. For this reason, the anatomical study was limited to osseous anatomical structures. The osseous anatomy, however, is most important when considering posterior spinal instrumentation. A surgeon placing pedicle screws at the apex level, for instance, should be aware that at the midpoint of the foramen at the pedicle isthmus (where the pedicle cortices are closest on either side of the foramen), the convex side will have a FH, FW, FA, and P-SAP larger by approximately 38%, 30%, 86%, and 47%, respectively, than the concave side. Although the relative importance of the intervertebral foramen anatomy is certainly secondary to that of the pedicle anatomy, which is clearly of cardinal importance to the scoliosis surgeon in planning instrumentation, this study contributes to the understanding of the local anatomy in AIS patients.

The foraminal size difference may give pause to think that if symptoms were ever to arise, a more thorough assessment of the implants on that side might be warranted. This could in theory influence selection of hardware for bony fixation, for example, use of a hook or wire construct rather than a screw in selected patients based on their individual circumstances. The authors did consider whether change in foraminal dimensions may be of clinical relevance in the event of pedicle breach into the foramen during placement of posteriorly inserted pedicle screws.

Although it would seem logical that the concavity thoracic nerve roots would be more at risk during posterior pedicle screw insertion from foraminal breach, this assertion is difficult to prove. Foraminal breaches (either superior or inferior pedicle breach into the foramen) are typically reported at low rates compared with medial or lateral breach. A systematic review by Hicks et al. [28] described inferior pedicle breaches in 14% of misplaced screws and superior breaches in 8% of misplaced screws. These rates however appear significantly higher than in many other studies in which foraminal breaches from pedicle screws are either not described at all [29-33] or at very low comparative or overall frequency [34,35].

Radicular symptoms or postoperative intercostal neuralgia are not widely reported in the literature as a complication of AIS deformity correction surgery [32,33,35]. The reasons for this are unclear; however, we speculate that the cross-sectional area of the foramen occupied by the thoracic root is sufficiently small such that breaches are generally well tolerated. An alternative explanation is that pedicle breaches into the foramen may be detected at time of surgery with subsequent re-siting of screws such that no breach is recorded on postoperative imaging and the patient has no clinical sequelae. Under these circumstances, the foraminal anatomy may be less relevant. The amount of foraminal compromise that can be tolerated by screw breach is unknown and would require more detailed studies.

The authors of this study are not advocating routine preoperative use of CT scans for the purpose of assessment of the intervertebral foramen in all patients; however, an appreciation for foraminal dimension differences may be obtained by the use of the data table in this study or if preoperative CT or magnetic resonance imaging scans of the spine have been obtained for other reasons.

The method for measurement of the foramina described in this study is reproducible on any desktop computer PACS system with a multiplanar reconstruction function. The opinion of the authors is that adjusting the axial plane in the manner described is an improvement on methods used in other studies and is more anatomically correct for examining the foramen.

Future Studies

This study did not measure volume of the intervertebral foramen. However, it is expected that the foramina on the concave side of the scoliotic curve are reduced in volume compared to the convex side because of the thinning of pedicles in the concavity. A study of this nature would require 3D modeling and would be difficult using low-dose CT data. Further studies that include patients with a wider range of Cobb angles and compare pre- and postoperative studies would be desirable. A study comparing differences in pedicle dimensions with foraminal dimensions would also help in understanding the relative contribution of pedicle deformity to altered foraminal dimensions.

Given the need to minimize radiation exposure in young patients, a comparison between CT and magnetic resonance imaging data would also be helpful.

Conclusions

Significant morphological differences exist in the intervertebral foramina in this CT study of 23 patients with AIS. As expected, the differences are quantitatively largest between the convex (right side) and concave (left side) at or near the apex of the major curve and appear to follow a predictable ratio according to position on the scoliosis curve. Surgeons undertaking scoliosis correction surgery should be aware of anatomical differences in the intervertebral foramina between the convexity and concavity.

References

[1] Hefti F. Pathogenesis and biomechanics of adolescent idiopathic scoliosis (AIS). *J Child Orthop* 2013;7:17−24.
[2] Parent S, Labelle H, Skalli W, et al. Morphometric analysis of anatomic scoliotic specimens. *Spine (Phila Pa 1976)* 2002;27:2305−11.
[3] Parent S, Labelle H, Skalli W, de Guise J. Thoracic pedicle morphometry in vertebrae from scoliotic spines. *Spine (Phila Pa 1976)* 2004;29:239−48.
[4] Sarwahi V, Sugarman EP, Wollowick AL, et al. Prevalence, distribution, and surgical relevance of idiopathic scoliosis vs. no deformity. *J Bone Joint Surg* 2014;92:1−8.
[5] Cinotti G, De Santis P, Nofroni I, Postacchini F. Stenosis of lumbar intervertebral foramen. *Spine (Phila Pa 1976)* 2002;27:223−9.
[6] Panjabi M, Duranceau J, Goel V. Cervical human vertebrae quantitative three-dimensional anatomy of the middle and lower regions. *Spine (Phila Pa 1976)* 1991;16:861−9.
[7] Panjabi M, Takata K, Goel V. Thoracic human vertebrae quantitative three-dimensional anatomy. *Spine (Phila Pa 1976)* 1991;16:888−901.
[8] Panjabi M, Goel V, Oxland T. Human lumbar vertebrae: quantitative three-dimensional anatomy. *Spine (Phila Pa 1976)* 1992;17:299−306.
[9] Panjabi MM, O'Holleran JD, Crisco JJ, Kothe R. Complexity of the thoracic spine pedicle anatomy. *Eur Spine J* 1997;6:19−24.
[10] Liljenqvist UR, Link TM, Halm HF. Morphometric analysis of thoracic and lumbar vertebrae in idiopathic scoliosis. *Spine (Phila Pa 1976)* 2000;25:1247−53.
[11] Makino T, Kaito T, Fujiwara H, Yonenobu K. Morphometric analysis using multiplanar reconstructed CT of the lumbar pedicle in patients with degenerative lumbar scoliosis characterized by a Cobb angle of 30° or greater. *J Neurosurg Spine* 2012;17:256−62.
[12] Ploumis A, Transfeldt EE, Gilbert TJ, et al. Degenerative lumbar scoliosis: radiographic correlation of lateral rotatory olisthesis with neural canal dimensions. *Spine (Phila Pa 1976)* 2006;31:2353−8.
[13] Ebraheim NA, Liu J, Shafiq Q, et al. Quantitative analysis of changes in cervical intervertebral foramen size with vertebral translation. *Spine (Phila Pa 1976)* 2006;31:E62−5.
[14] Evangelopoulos D. Computerized tomographic morphometric analysis of the cervical spine. *Open Orthop J* 2012;6:250−4.
[15] Kaneko Y, Matsumoto M, Takaishi H, et al. Morphometric analysis of the lumbar intervertebral foramen in patients with degenerative lumbar scoliosis by multidetector-row computed tomography. *Eur Spine J* 2012;21:2594−602.
[16] Fujiwara A, An HS, Lim TH, Haughton VM. Morphologic changes in the lumbar intervertebral foramen due to flexion-extension, lateral bending, and axial rotation: an in vitro anatomic and biomechanical study. *Spine (Phila Pa 1976)* 2001;26:876−82.

[17] Inufusa A, An H, Lim T, Hasegawa T. Anatomic changes of the spinal canal and intervertebral foramen associated with flexion-extension movement. *Spine (Phila Pa 1976)* 1996;21:2412−20.

[18] Yuan C, Zhu H, Song D, et al. Impact and clinical significance of pedicle length on spinal canal and intervertebral foramen area. *Int J Clin Exp Med* 2014;7:163−9.

[19] Osman S, Nibu K, Panjabi M. Transforaminal and posterior decompressions of the lumbar spine: a comparative study of stability and intervertebral foramen area. *Spine (Phila Pa 1976)* 1997;22:1690−5.

[20] Smith G, Aspden R, Porter R. Measurement of vertebral foraminal dimensions using three-dimensional computerized tomography. *Spine (Phila Pa 1976)* 1993;18:629−36.

[21] Vrtovec T, Pernus F, Likar B. A review of methods for quantitative evaluation of axial vertebral rotation. *Eur Spine J* 2009;18:1079−90.

[22] Vrtovec T, Pernus F, Likar B. A review of methods for quantitative evaluation of spinal curvature. *Eur Spine J* 2009;18:593−607.

[23] Krag M, Weaver D, Beynnon B, Haugh L. Morphometry of the thoracic and lumbar spine related to transpedicular screw placement for surgical spinal fixation. *Spine (Phila Pa 1976)* 1988;13:27−32.

[24] Misenhimer G, Peek R, Wiltse L. Anatomic analysis of pedicle cortical and cancellous diameter as related to screw size. *Spine (Phila Pa 1976)* 1989;14:367−72.

[25] Xiong B, Sevastik B, Sevastik J, et al. Horizontal plane morphometry of normal and scoliotic vertebrae—a methodological study. *Eur Spine J* 1995;4:6−10.

[26] Bland JM, Altman DG. Applying the right statistics: analyses of measurement studies. *Ultrasound Obstet Gynecol* 2003;22:85−93.

[27] Lee WT, Cheung CS, Tse YK, et al. Association of osteopenia with curve severity in adolescent idiopathic scoliosis: a study of 919 girls. *Osteoporos Int* 2005;12:1924−32.

[28] Hicks JM, Singla A, Shen FH, Arlet V. Complications of pedicle screw fixation in scoliosis surgery: a systematic review. *Spine (Phila Pa 1976)* 2010;35:E465−70.

[29] Modi HN, Suh SW, Fernandez H, et al. Accuracy and safety of pedicle screw placement in neuromuscular scoliosis with free-hand technique. *Eur Spine J* 2008;17:1686−96.

[30] Modi H, Suh SW, Song HR, Yang JH. Accuracy of thoracic pedicle screw placement in scoliosis using the ideal pedicle entry point during the freehand technique. *Int Orthop* 2009;33:469−75.

[31] Sarlak AY, Tosun B, Atmaca H, et al. Evaluation of thoracic pedicle screw placement in adolescent idiopathic scoliosis. *Eur Spine J* 2009;18:1892−7.

[32] Kuklo TR, Lenke LG, O'Brien MF, et al. Accuracy and efficacy of thoracic pedicle screws in curves more than 90 degrees. *Spine (Phila Pa 1976)* 2005;30:222−6.

[33] Samdani AF, Ranade A, Sciubba DM, et al. Accuracy of free-hand placement of thoracic pedicle screws in adolescent idiopathic scoliosis: How much of a difference does surgeon experience make? *Eur Spine J* 2010;19:91−5.

[34] Di Silvestre M, Parisini P, Lolli F, Bakaloudis G. Complications of thoracic pedicle screws in scoliosis treatment. *Spine (Phila Pa 1976)* 2007;32:1655−61.

[35] Suk SI, Kim WJ, Lee SM, et al. Thoracic pedicle screw fixation in spinal deformities: are they really safe? *Spine (Phila Pa 1976)* 2001;26:2049−57.